Eur. Phys. J. D **38**, 299–306 (2006)
DOI: 10.1140/epjd/e2006-00005-7

THE EUROPEAN PHYSICAL JOURNAL D

Fragmentation and ionization of C_{70} and C_{60} by slow ions of intermediate charge

H. Zettergren[1,a], P. Reinhed[1], K. Støchkel[1], H.T. Schmidt[1], H. Cederquist[1], J. Jensen[2], S. Tomita[3], S.B. Nielsen[4], P. Hvelplund[4], B. Manil[5], J. Rangama[5], and B.A. Huber[5]

[1] Physics Department, Stockholm University, AlbaNova University Center, 10691 Stockholm, Sweden
[2] Division of Ion Physics, Ångström Laboratory, Uppsala University, Box 534, 75121 Uppsala, Sweden
[3] Institute of Applied Physics, University of Tsukuba, Tsukuba, Ibaraki 305-0006, Japan
[4] Department of Physics and Astronomy, University of Aarhus, 8000 Aarhus C, Denmark
[5] CIRIL/GANIL, rue Claude Bloch, B.P. 5133, 14070 Caen Cedex 05, France

Received 26 August 2005 / Received in final form 9 November 2005
Published online 10 January 2006 –

Abstract. We have measured total and coincident (with outgoing charge-state analyzed projectiles) ionization and fragmentation spectra of C_{60} and C_{70} following collisions with Xe^{4+} and Kr^{4+} at $v = 0.06$ a.u. Intact positive fullerene ions in charge states up to five (C_{60}^{5+} and C_{70}^{5+}) are produced with both projectiles and for Kr^{4+}+C_{70} collisions we even observe a small C_{70}^{6+} peak. The $C_{60/70-2m}^{3+}$ ($m = 1$–7) intensity distributions are predominantly associated with the stabilization of three electrons on the projectile ($s = 3$) and are significantly different for Xe^{4+}- and Kr^{4+}-projectiles. On the other hand, we find remarkable similarities in the C_3^+-C_{11}^+ multi-fragmentation pattern regardless of projectile species (mass) although they are associated with closer encounters in which the projectile is fully neutralized ($s = 4$). Simple Monte Carlo calculations of nuclear and electronic loss processes show that both these contributions are very similar in glancing Xe^{4+}+C_{60} and Kr^{4+}+C_{60} collisions, suggesting that frontal (and more violent) collisions are strongly suppressed under the present experimental conditions. Nevertheless it is surprising that the more distant collisions ($s = 3$) are projectile mass dependent, while the closer collisions ($s = 4$) are not. This indicates that this simple approach (although it reproduces more advanced quantum mechanical calculations for slow collisions with *singly* charged atomic ions rather well) is not valid for a comprehensive description of the energy transfer processes in the present collision systems involving projectiles of higher charge states.

PACS. 34.70.+e Charge transfer – 36.40.Qv Stability and fragmentation of clusters – 36.40.Wa Charged clusters

1 Introduction

Since the last decade, ionization, excitation, charge transfer, and fragmentation of fullerenes (in particular C_{60}) have been the subjects of numerous theoretical and experimental studies (see e.g. [1,2] and references therein). Experimentally, these reactions have been studied in collisions with atomic, molecular, and cluster ions, as well as with electrons and photons. Nowadays, coincidence techniques are often used to determine e.g. the reaction pathways, branching ratios, and kinetic energy releases in the fragmentation processes [3–6].

It is well-established that slow highly charged ions capture electrons at rather large distances in accordance with the classical over-the-barrier model [5,7–9]. In these processes it is expected that small amounts of energy are transferred to the fullerene ion, leading mainly to electronic excitations which subsequently will be transferred into the vibrational modes (on a timescale longer than the collision time).

In a recent study, members of the present collaboration reported on the first detailed ionization and fragmentation study of C_{60} and *purified* C_{70} in collisions with slow *highly* charged ions [10]. In the present work we analyze fragment ion mass spectra and the related kinetic energy releases for two *intermediate charge-state* projectiles (Xe^{4+}, Kr^{4+}) at $v = 0.06$ a.u., yielding results for Xe^{4+}+C_{60}, Kr^{4+}+C_{60}, Xe^{4+}+C_{70}, and Kr^{4+}+C_{70}. In addition, we have measured the fragmentation features for Xe^{4+}+C_{60} at a higher velocity ($v = 0.078$). Here, we focus the discussion on the comparisons of various fragmentation features and their dependencies on the projectile species (Xe^{4+} or Kr^{4+}), fullerene size (C_{60} or C_{70}), and collision velocity. These comparisons reveal some rather surprising features such

[a] e-mail: henning@physto.se

as insensitivities to the projectile species (mass) and target size (C_{60} or C_{70}) for the production of small carbon clusters in the (C_3^+-C_{11}^+)-mass range. In seeming contrast to these observations we record a clear projectile-mass influence on the relative $C_{60/70-2m}^{3+}$ distributions, which we show are due to collisions at larger distances than those yielding the (C_3^+-C_{11}^+)-ions. We discuss these findings in terms of an earlier developed Monte Carlo model for nuclear and electronic energy transfer to the target [5]. In spite of some obvious shortcomings of this model, which will be discussed below, we use it for the present collision systems and for Ar^++C_{60} collisions at $v = 0.04$–0.45 a.u. For the latter case we find rather good agreement with the full quantal calculations of Kunert and Schmidt [11] indicating that our model [5] can be used as a basis for discussion of nuclear and electronic energy transfers for slow ions of low charge states. In this work, however, we argue that such a model is too crude to catch the essentials of energy transfer processes for multiply charged projectiles.

The present fragmentation kinetic energy release measurements and coincidence measurements for given numbers of electrons (s) stabilized on the projectile allow us to deduce details of the fragmentation pathways. We are, for instance, able to discriminate between fragmentation sequences such as [mC_2] (pure C_2 evaporation), [$(m-1)C_2$+C_2^+], [$(m-2)C_2$+C_4^+], and [$(m-3)C_2$+C_6^+] where the latter three include emissions of one C_2^+-, one C_4^+-, and one C_6^+-molecule, respectively. From these results we then deduce the initial fullerene charge state distributions and find that the higher fullerene charge states are more efficiently produced by Kr^{4+} at $v = 0.06$ a.u. than by Xe^{4+} at the same velocity. This result is further underscored by the appearance of doubly charged C_{15}^{2+}-C_{23}^{2+} fragments for the Kr^{4+}+C_{60} collision system. We believe that the C_{15}^{2+}-C_{23}^{2+}-peaks are signatures of multi-fragmentation of fullerene ions in high charge states (C_{60}^{r+} with $r \geq 5$).

2 Experimental techniques

The experimental procedure has been discussed in detail elsewhere [12,13], and only a brief description is given here. A schematic of the experimental setup is shown in Figure 1. The Xe^{4+}- and Kr^{4+}-projectiles were extracted at 3–5q and 1.9q keV, respectively, using the 14.5 GHz Electron Cyclotron Resonance (ECR) ion source at the Manne Siegbahn Laboratory, Stockholm University. The ion beams were transported to the experimental set-up, where they crossed collimated jets of either C_{70} or C_{60}, effusing from a small oven. The interaction region lay in the extraction stage of a linear time-of-flight (TOF) mass spectrometer, and the fullerene jets pointed in the direction of the spectrometer axis. The temperature of the oven was set to 600 °C for both targets. The C_{60} and C_{70} powders had purities of 99.9% and 99.4% (Hoechst), respectively (0.4% of the C_{70} powder consist of C_{60}, the rest contains higher fullerenes). The oven was carefully cleaned between target changes.

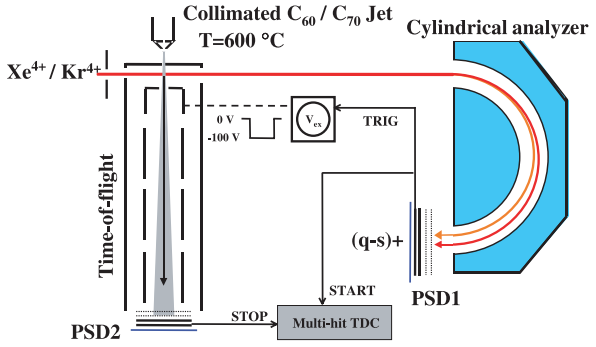

Fig. 1. Schematic of the experimental setup in the coincidence measurement mode (cf. text).

Two different techniques were used to record the total and coincidence fragment ion mass spectra. First, the projectile beam was pulsed at 2 kHz with a 10 μs pulse duration. Intact and fragment ions were extracted with a transverse electric-field, applied immediately after the beam pulse had passed through the target jet. This means that the time from the creation of the ions to the extraction was limited to 10 μs. In the second (coincidence) mode, the projectile charge state was selected by means of a 180° electrostatic cylindrical analyzer followed by a position sensitive detector. Here, the extraction was triggered by a fast signal from this detector. Thus the time from the creation of the fragment ions to the extraction equals the projectile flight time from the interaction region to the projectile detector (∼5.5 μs). In both modes, the extracted ions transverse the TOF before hitting a position sensitive detector (50 mm diameter). The time-of-flight measurements were started with the extraction signal and stopped with the target ion signal. An event-by-event acquisition system was used to store the data. Each time-of-flight peak is associated with a position distribution on the recoil detector characteristic for Kinetic Energy Releases (KER) in the post-collisional fragmentation process. The method to extract KER-values has been discussed in detail earlier [12,13].

3 Results and discussion

In Figure 2 we show the *total* ion mass spectra (using the 2 kHz pulsed extraction technique) for our four collision systems at $v = 0.06$ a.u. The distributions of intensities of intact fullerenes are to large extents similar in all cases. However, there are also slight preferences for higher charges of intact fullerenes for Kr^{4+}- than for Xe^{4+}-projectiles and for the C_{70}- in comparison with the C_{60}-target. There are strong projectile dependences for the C_{60-2m}^{3+} and C_{70-2m}^{3+} fragment distributions, while the m-dependence of C_{60-2m}^{3+} strongly resembles the one for C_{70-2m}^{3+} for a given projectile. In Figure 3 we show zoomins of the light fragments (C_3^+-C_{12}^+) in the total spectra. The C_3^+-C_{11}^+ distributions are similar on strikingly detailed levels for Xe^{4+}+C_{70}, Xe^{4+}+C_{60}, Kr^{4+}+C_{70}, and

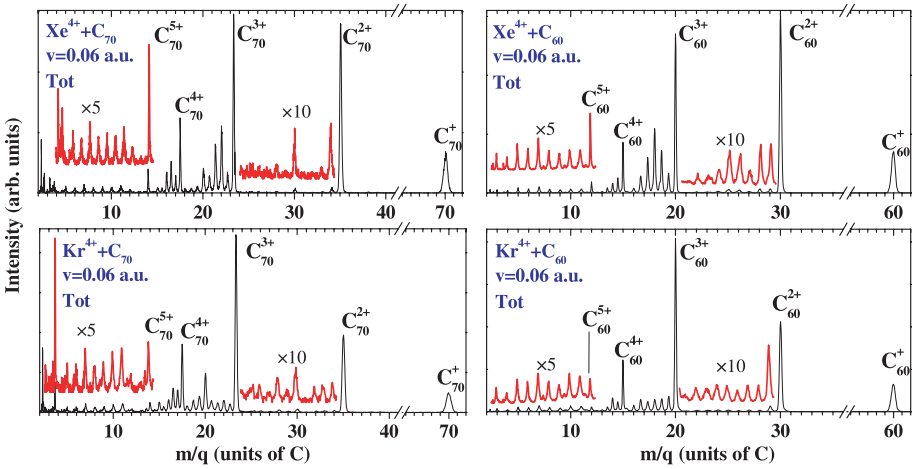

Fig. 2. The *total* ion mass spectra (extraction at fixed frequency 2 kHz and the 10 μs pulse length) due to 12 keV Xe^{4+}+C_{70} collisions (upper left), 12 keV Xe^{4+}+C_{60} collisions (upper right), 7.6 keV Kr^{4+}+C_{70} collisions (lower left), and 7.6 keV Kr^{4+}+C_{60} collisions (lower right). The collision velocity is the same in all four cases ($v = 0.06$ a.u.).

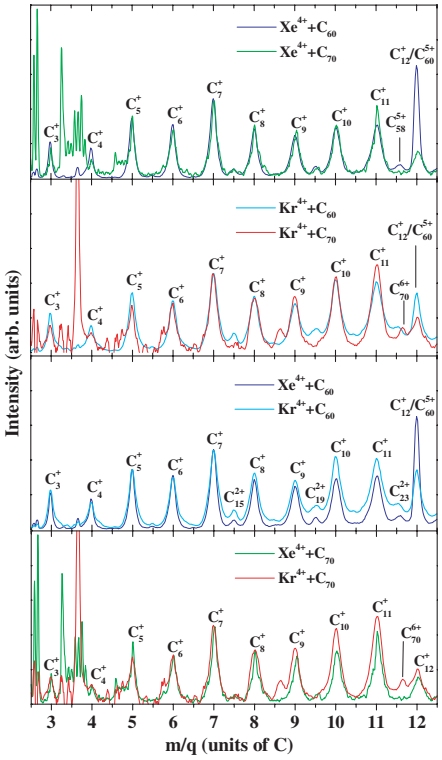

Fig. 3. Detailed views of small fragment peaks in the total mass spectra. The large peaks in the C_{70} cases for $m/q < 4$ are due to collisions with residual gas. C^+ and C_2^+ are also detected for all cases, but not shown due to interfering background peaks. The small peak at about $m/q = 8.6$ in the Kr^{4+}+C_{70} case is due to background.

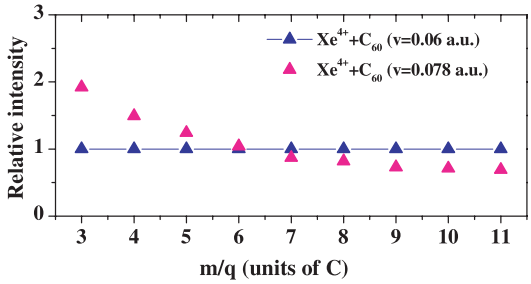

Fig. 4. The relative intensities of the small fragments in 12 and 20 keV Xe^{4+}+C_{60} collisions ($v = 0.06$ a.u. and $v = 0.078$ a.u.) normalized to the results at $v = 0.06$ a.u.

Kr^{4+}+C_{60} collisions. The comparison for Xe^{4+}+C_{60} and Xe^{4+}+C_{70} in the top panel of Figure 3 show remarkable similarities to the extent that they are close to being identical with the exception of C_{11}^+ for which a small difference is observed. Thus, the Xe^{4+}+C_{60} and Xe^{4+}+C_{70} collisions creating the (C_3^+-C_{11}^+) mass distributions transferred similar energies per internal vibrational degree of freedom for C_{60} and C_{70}. For Kr^{4+}+C_{60} and Kr^{4+}+C_{70} collisions (second panel of Fig. 3) we also find large similarities for the light singly charged fragments, but an enhanced production of doubly charged ions, C_{15}^{2+}-C_{23}^{2+} in the C_{60} case. Note that the even-numbered doubly charged fragments (C_{16}^{2+}, C_{18}^{2+}, C_{20}^{2+}, C_{22}^{2+}) most likely are responsible for the broadening of the $m/q = 8$–11 peaks for Kr^{4+}+C_{60}. These doubly charged fragments are also responsible for the small differences in the third panel of Figure 3 and we infer that the singly charged fragment distributions are very similar for Xe^{4+} and Kr^{4+} impact at $v = 0.06$ a.u. In the lowest panel of Figure 3 we see that small amounts of C_{70}^{6+} are created in Kr^{4+}+C_{70} collisions, which again shows that Kr^{4+} is more efficient than Xe^{4+} in creating intact fullerenes in high charge states.

In Figure 4 we show the intensities of the C_3^+-C_{11}^+ peaks at $v = 0.078$ a.u. in comparison with the intensities of the corresponding peaks at $v = 0.06$ a.u. There is a clear enhancement of the lower mass peaks with increasing velocity indicating that electronic processes are important.

In Figure 5 we show comparisons of three total recoil ion mass spectra (cf. Fig. 2) and the corresponding mass

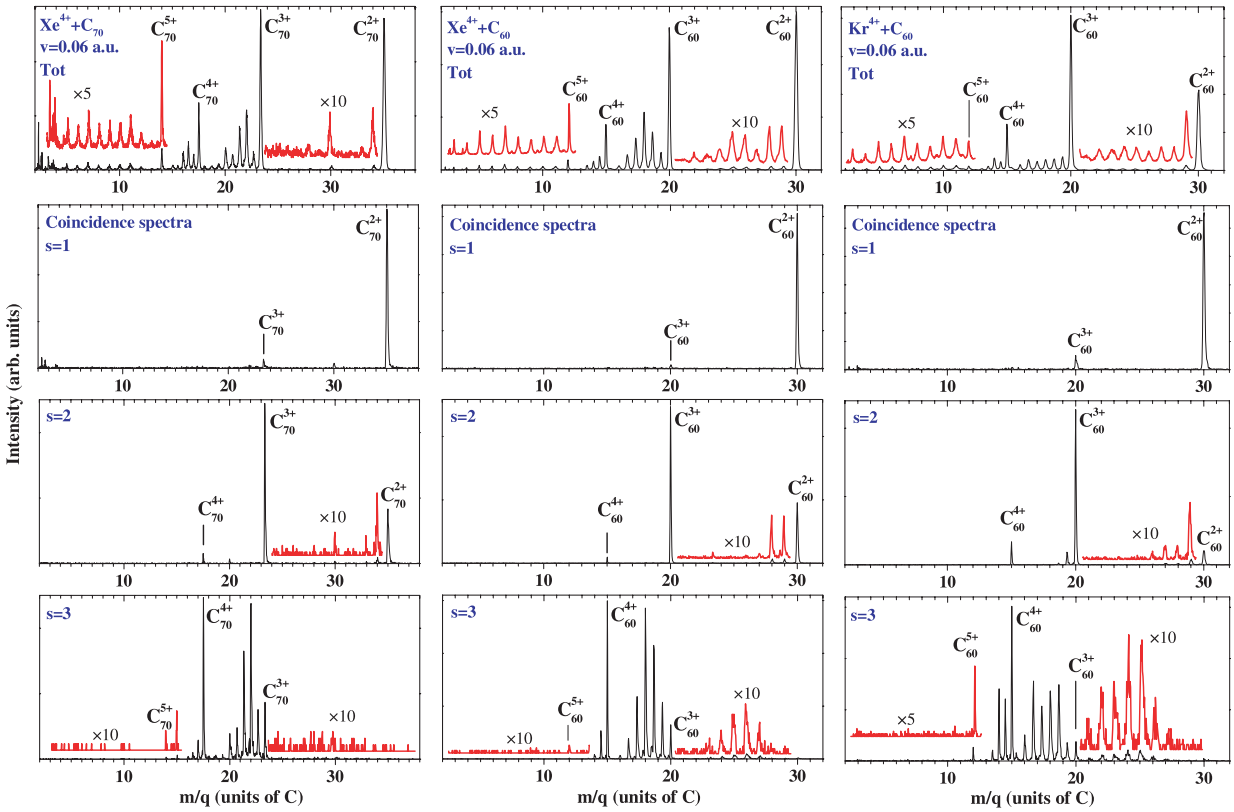

Fig. 5. Mass spectra of the collision products from 12 keV Xe^{4+}+C_{70} (left column), 12 keV Xe^{4+}+C_{60} (middle column), and 7.6 keV Kr^{4+}+C_{60} collisions (right column). The first row displays the total spectra, while the remaining rows display the mass distributions of intact and fragmented fullerene ions in coincidence with $s = 1$, 2, and 3 electrons stabilized on the Xe^{4+}/Kr^{4+} projectiles. Note that the singly charged intact peaks in the total and the $s = 1$ spectra are not shown.

spectra recorded in coincidence with $s = 1$, 2, and 3 electrons stabilized on the projectile. We note that:

(i) only intact fullerenes are created in processes for which one electron is stabilized on the projectile ($s = 1$);

(ii) mostly intact fullerenes are created for $s = 2$, but there are small contributions from evaporation of small carbon clusters for all three cases with C_{60}^{2+} and C_{70}^{2+} while there is evaporation from three times charged fullerenes only for Kr^{4+}+C_{60} when $s = 2$;

(iii) for $s = 3$ we note that C_{60}^{3+} both evaporates and undergoes fission (charged fragment emission), but that evaporation dominates. The C_{70}^{3+} only evaporates;

(iv) the C_{60}^{4+}- and C_{70}^{4+}-ions evaporate and decay by processes including fission;

(v) the C_{60}^{5+}- and C_{70}^{5+}-peaks are rather weak in $s = 3$ although they are strong in the total spectra. The latter shows that C_{60}^{5+}- and C_{70}^{5+}-productions are dominated by processes in which the projectiles are fully neutralized;

(vi) no fragments in the range C_3^+-C_{12}^+ are observed in the coincidence spectra and we conclude that these fragments only appear when the projectiles are neutralized.

The fragment- and intact-ion position-distribution widths [12,13] for the peaks in the *total* mass spectra (cf. Fig. 2) are shown in Figure 6. We note that the latter distributions are narrow and independent of projectile species (Xe^{4+} or Kr^{4+}), while the $C_{58/68}^{2+}$ widths (2D fragment images are shown in the upper part of Fig. 6) are only slightly larger and typical for single-step evaporation processes (neutral C_2 emission from $C_{60/70}^{2+}$). The lower solid curves are calculated lower limits for the recoil widths for sequences of neutral C_2-emissions where we assume that kinetic energy releases for each subsequent step $C_{58}^{2+} \rightarrow C_{56}^{2+} + C_2$, $C_{56}^{2+} \rightarrow C_{54}^{2+} + C_2$, etc. are the same as for the initial step $C_{60}^{2+} \rightarrow C_{58}^{2+} + C_2$. This leads to a kinetic energy release scaling as $\sqrt{m}$ for sequential emission of m C_2-units. From the comparison between this curve and the measured C_{56}^{2+} and C_{66}^{2+} widths we conclude that the $C_{56/66}^{2+}$-peaks stem from two-step evaporation ($C_2 + C_2$). The second lowest solid curves display the widths corresponding to fragmentation sequences $[(m-1)C_2 + C_2^+]$. The broadening of the recoil distribution in the fission step was determined from the kinetic energy released in the binary process, $C_{60}^{3+} \rightarrow C_{58}^{2+} + C_2^+$, as recently calculated by means of high level Density Functional Theory by Díaz-Tendero et al. [14]. Similarly, the two upper solid curves in the right part of Figure 6 correspond to $[(m-2)C_2+C_4^+]$- and $[(m-3)C_2 + C_6^+]$-sequences, respectively. The measured widths in the total Xe^{4+} + C_{60} and Kr^{4+} + C_{60} spectra

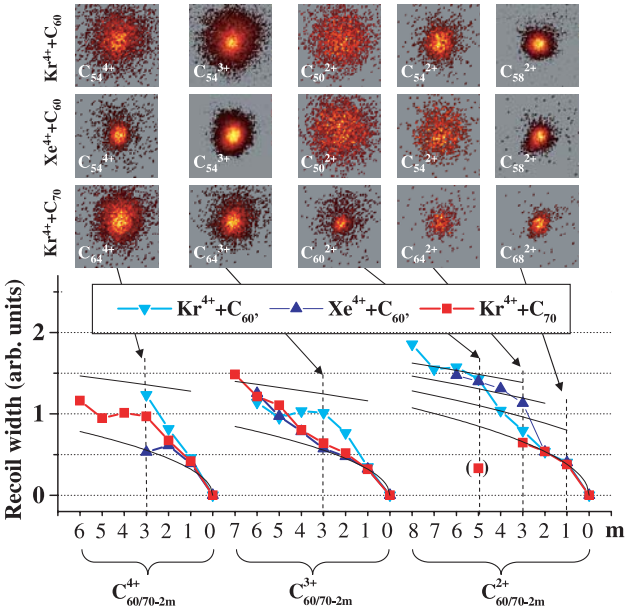

Fig. 6. The widths of the fragment detector images of the intact ($m = 0$) and fragmented ($m \geq 1$) fullerene ions produced in Kr^{4+}+C_{60}, Xe^{4+}+C_{60}, and Kr^{4+}+C_{70} collisions (total spectra). A few two-dimensional detector images are shown in the upper part. The solid curves show (from bottom to top) expected widths for sequential $[mC_2]$-, $[(m-1)C_2+C_2^+]$-, $[(m-2)C_2+C_4^+]$-, and $[(m-3)C_2+C_6^+]$-decay.

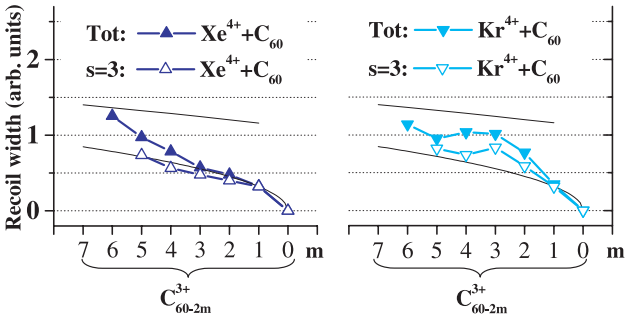

Fig. 7. The widths (solid triangles: from the total spectra; open triangles: from the $s = 3$ coincidences) of the fragment detector images for Xe^{4+} + C_{60} (left) and Kr^{4+} + C_{60} collisions (right). Solid curves: $[mC_2]$ and $[(m-1)C_2 + C_2^+]$ decay sequences (cf. text).

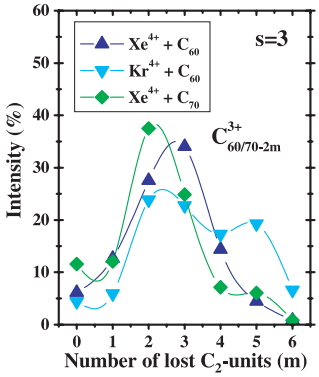

Fig. 8. The triply charged fragment peak distributions in the coincidence fragment ion mass spectra ($s = 3$) for $Xe^{4+} + C_{60}$, $Kr^{4+} + C_{60}$, and $Xe^{4+} + C_{70}$.

for C^{2+}_{60-2m} with $m \geq 3$ (Xe^{4+}) and $m \geq 5$ (Kr^{4+}) mostly fall between these two upper curves, indicating that C_4^+/C_6^+ indeed are involved in the emission sequences [15, 16]. It should be noted that the correlation between two small charged fragments and one large fragment ion has *not* been observed for low parent ion charge states [15], supporting the idea that the large widths of the lighter C^{2+}_{60-2m} fragments observed are due to emission of one heavier charged fragment (C_4^+ or C_6^+) rather than two (or more) C_2^+ fragments. In the Kr^{4+} + C_{70} case, the C^{2+}_{60}-fragment width falls below the evaporation limit (solid curve) due to small amounts of contaminant-C_{60} in the C_{70} powder.

All triply charged fragments in the total spectra (except $m = 7$ in the Kr^{4+} + C_{70} case) lie between the sequential fragmentation curves corresponding to $[mC_2]$- and $[(m-1)C_2+C_2^+]$-decays. Contributions from fission appears for C^{3+}_{60-2m} ($m \geq 2$) in the $Kr^{4+} + C_{60}$ case, and for $C^{3+}_{60/70-2m}$ ($m \geq 4$) in the other two cases. Earlier, fragment-fragment coincidence studies of C^{4+}_{60} created in collisions with H^+ [15], Ar^{8+} [17], and Xe^{25+} [18] show that the dominating fission channel involves C_4^+-emission, but also C_6^+ fragments were found in coincidence with C^{3+}_{48}-C^{3+}_{52} fragments [15]. As discussed above, these processes would lead to significantly larger recoil widths than those actually observed here (cf. Fig. 6). We therefore conclude that the major part of the triply charged fragments in the present *total* fragment spectra (Fig. 2) originate from (sequential) $[mC_2]$-evaporation of C^{3+}_{60}. Repeating the same argument for the quadruply charged fragments, all peaks are dominated by evaporation except C^{4+}_{54} in the Kr^{4+}+C_{60} case, which has a significant contribution from the $[C^{5+}_{60} \rightarrow C^{4+}_{54} + 2C_2 + C_2^+]$-sequence.

The position widths for the Xe^{4+} + C_{60} $\rightarrow$ Xe^+ + C^{3+}_{60-2m} *coincidence* events (cf. Fig. 7), are consistent with pure neutral $[mC_2]$-emission sequences. For the Kr^{4+} + C_{60}, ($s = 3$)-coincidences there are only minor contributions from fission. Thus, the fragment distributions in Figure 8 show the relative intensities (as functions of m) for the products of the $Xe^{4+}/Kr^{4+} + C_{60} \rightarrow Xe^+/Kr^+ + C^{3+}_{60-2m} + mC_2$ and $Xe^{4+} + C_{70} \rightarrow Xe^+ + C^{3+}_{70-2m} + mC_2$ evaporation sequences. We see that the target dependence on the shapes of the distributions is rather weak compared to the markedly different C^{3+}_{60-2m} distributions for Xe^{4+}- and Kr^{4+}-projectiles, and that all three deviate from the typical behavior of evaporative sequences [19]. This is rather surprising as the parent ions from a classical over-the-barrier point of view would be expected to be created at rather large impact parameters where energy transfers should be small. Obviously this is not the case and the amounts of energy required to induce such long sequences of evaporation suggest that simple "stopping-power based" descriptions of energy transfer are inadequate for collisions involving multiply charged ions.

In contrast to highly charged projectiles [5,7–9,20,21], projectiles in intermediate charge states capture electrons into low lying electronic states where the quasicontinuum condition may not be fulfilled. That is, there is not always an available resonant projectile state to be captured to at the critical over-the-barrier distances. Thus, the critical distances $R_1 = 23.6a_0$, $R_2 = 20.5a_0$, $R_3 = 17.8a_0$, and $R_4 = 15.1a_0$ for transfer of one, two, three, and four electrons from C_{60} are upper limits for the electron transfer distances. As transfer of four electrons appears to be possible at distances far outside the fullerene radius very little energy transfer would be expected from a stopping power approach [5]. However, the present total and coincidence ion-mass spectra unambiguously show that substantial energy transfers are associated with collisions in which three, four, or five electrons are removed from the fullerene target.

We used a Monte Carlo method [5] to calculate the nuclear and electronic stopping for large sets of randomly generated impact parameters and orientations of the fullerene cage. These energy transfers are obtained as the sum of 60 individual energy transfer for carbon *atoms* placed in the C_{60} geometry. The electronic stopping is given by the Firsov formula [22], while the nuclear part is computed using a screened Bohr potential. It should be noted that the cage structure is static in the present simulations. As a consequence, the nuclear energy transfer is overestimated in frontal collisions, while the electronic part is overestimated for impacts near the cage due to the increased electron density from the individual carbon atoms in comparison with the more extended electron cloud of the real C_{60} fullerene. This also means that the electronic stopping is underestimated at somewhat larger distances. However, applying the present method to $Ar^+ + C_{60}$ collisions we obtain results close to the non-adiabatic quantum molecular dynamic simulations by Kunert and Schmidt [11] showing that our model still may be useful for crude estimates of the stopping power in close collisions and for projectiles in the lowest charge states.

In Figure 9, we show the electronic and nuclear stopping for impact parameter intervals corresponding to frontal collisions (b = 0–7a_0) and impacts outside the cage but inside the limit b_{max} for direct knock out processes ($b = 7a_0$–b_{max}), where we follow Larsen et al. [23] and calculate b_{max} for 13.5 eV energy transfer in binary Kr+C and Xe+C collisions yielding $b_{max} = 9.3a_0$ and $b_{max} = 9.8a_0$, respectively. In frontal collisions energy transfers are found to be rather strongly dependent on the mass and the velocity of the projectile (cf. Fig. 9). This basically rules out the possibility that the present C_3^+-C_{11}^+ mass distribution, with their observed independence of projectile mass at $v = 0.06$ a.u., could be due to frontal collisions. Further, substantial amounts of energies (of the order of keV) are transfered in all direct hits, which lead to almost complete destruction of the fullerene cage. In glancing collisions ($b = 7a_0$–b_{max}), on the other hand, the corresponding energy distributions are much more similar for Kr and Xe at $v = 0.06$ a.u. This is consistent with a

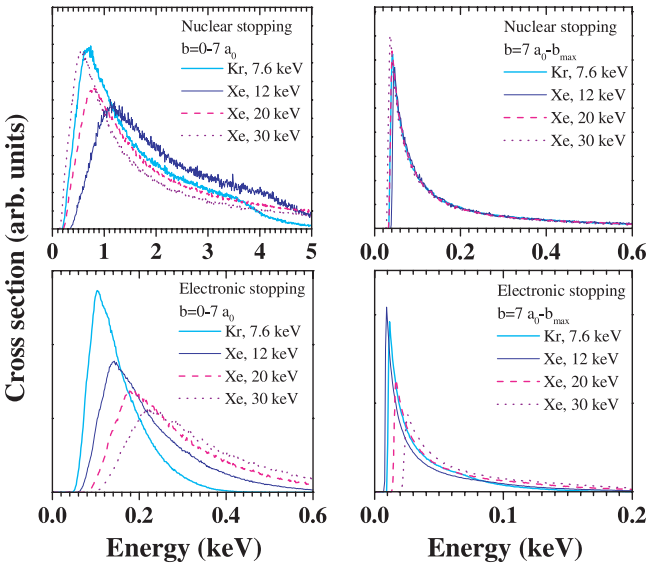

Fig. 9. Monte Carlo calculations of electronic and nuclear stopping in direct (b = 0–7a_0) and glancing ($b = 7a_0$–b_{max}) X + C_{60} collisions (X = 7.6 keV Kr, 12 keV Xe, 20 keV Xe, and 30 keV Xe).

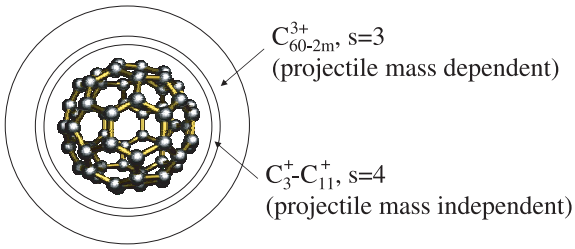

Fig. 10. Schematic of the collision regions associated with the observed projectile mass independent C_3^+-C_{11}^+ distributions and projectile mass dependent $C_{60/70}^{3+} \rightarrow C_{60/70-2m}^{3+} + mC_2$ evaporative sequences. In these processes, $s = 4$ and $s = 3$ electrons are stabilized on the projectile, respectively.

picture in which glancing collisions are responsible for the C_3^+-C_{11}^+ fragment distributions and their insensitivities to the projectile mass. The importance of glancing collisions for the C_3^+-C_{11}^+ distribution is further underscored by the fact that they always lead to the complete neutralization of the projectile ($s = 4$).

However, this crude calculation of energy transfer to the fullerenes is obviously not appropriate for descriptions of energy transfers in somewhat more distant collisions with multiply charged ions. In the present cases, the more distant collisions yield the C_{60-2m}^{3+} and C_{70-2m}^{3+} distributions from post collisional C_2-evaporation from C_{60}^{3+} and C_{70}^{3+} and are rather strongly dependent of the projectile mass (cf. Fig. 10). This indicates that it is necessary to also take electronic excitations induced in the ionization processes into account, which would require similar calculations as those performed by Kunert and Schmidt [11] also for multiply charged projectiles.

In Figure 11 we show the relative charge state distributions for C_{60}- and C_{70}- fullerenes before and after the

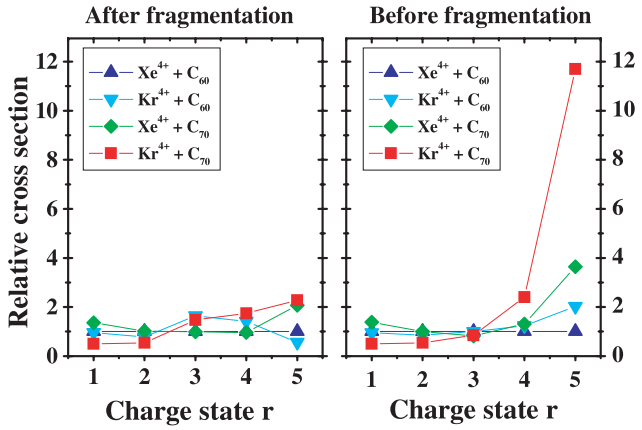

Fig. 11. Left: the relative cross-sections for producing C_{60}^{r+} and C_{70}^{r+} ions which are stable on the time scale of the measurement. The cross-section are normalized to the $Xe^{4+} + C_{60}$ results. Right: the corresponding distributions before fragmentation, reconstructed from the information given by the fragment distributions. Lines are drawn to guide the eye.

respective fragmentation processes. The former data were obtained with the aid of the kinetic energy release measurements by which fragmentation pathways could be deduced. From Figure 11 it is clear that the Kr^{4+}-projectile is more efficient than Xe^{4+} in producing highly charged fullerenes. The production of intact C_{70}^{6+} in Kr^{4+}-collisions is not shown here but is clearly visible in Figure 3.

The formation of a target charge state exceeding the incident projectiles charge state has been observed before using H^+ [6], $He^{1+,2+}$- [24,25], O^{q+}- $(1 \leq q \leq 5)$ [26], $Ar^{1+,2+}$-projectiles [27–29]. Nevertheless, it is rather surprising in the present study as direct ionization processes are negligible for low impact velocities. Penning ionization has been proposed to contribute in very slow $Ar^{1+,2+}$ projectiles [28,29]. On the other hand, Martin et al. [21,30] have shown that many more electrons than the initial charge state of the projectile are ejected in (highly) charged ion-fullerene collisions, which was explained by a fast de-excitation mechanism during the interaction time. However, these processes have not been observed with Ar^{8+} projectiles and are thus most likely inactive in the present systems as the projectiles (Xe^{4+} and Kr^{4+}) have even lower potential energies. Although the formation mechanism still is an open question, it is clear from the present study that the cross-section for "over-charging" of the target depends on the mass and/or electronic structure of the projectile.

4 Summary and conclusions

We have investigated the ionization and fragmentation of C_{60} and C_{70} following collisions with Xe^{4+}- and Kr^{4+}-projectiles at $v = 0.06$ a.u. using two complementary experimental methods. We find a significant projectile-species sensitivity in the C_{60-2m}^{3+} $(m = 1–7)$ distributions as it is different for Xe^{4+} and Kr^{4+}-impact. A very similar difference also appears for the C_{70-2m}^{3+} distributions emphasizing that this is indeed linked to the nature of the projectile (electronic structure and/or mass).

When comparing the intensity distributions for C_3^+-C_{11}^+ fragments we find a most remarkable similarity for $Xe^{4+} + C_{60}$ and $Xe^{4+} + C_{70}$ collisions. As these two distributions are basically identical we conclude that the relative intensities on C_3^+-C_{11}^+ are dictated by the binding energy per atom for these small species and that the collision events are associated with similar amounts of energies deposited per internal vibrational degree of freedom in the C_{60} and C_{70}. The relative intensity distributions within the C_3^+-C_{11}^+ mass range are also very similar for $Kr^{4+} + C_{60}$ and $Kr^{4+} + C_{70}$ collisions, but in the case of $Kr^{4+} + C_{60}$ new peaks due to the doubly charged fragments C_{15}^{2+}-C_{23}^{2+} appear. The weaknesses of the C_{15}^{2+}-C_{23}^{2+} peaks for collisions with C_{70} is most likely due to more efficient charge separation on the surface of a C_{70}- than on a C_{60}-target, while their absence for $Xe^{4+} + C_{60}$ collisions is related to the smaller tendency to produce highly ionized C_{60} than with Kr^{4+} projectiles.

Monte Carlo calculations of nuclear and electronic stopping power in *frontal* Kr^{4+}/Xe^{4+}+C_{60} collisions at $v = 0.06$ a.u. shows that energy transfers typically are in the keV range, and are rather different for the Xe^{4+} and the Kr^{4+}-collisions. The latter rules out the possibility that such frontal collisions could be the origin of the observed C_3^+-C_{11}^+ fragment distributions. By finding the smallest distances at which direct knock-out processes become impossible we define glancing collision impact parameter regions extending from just outside the cage ($7a_0$) out to $9.8a_0$ (Xe^{4+}) and $9.3a_0$ (Kr^{4+}) and calculate almost identical relations between energy transfer and impact parameter.

From these calculations we rationalize the observation of a large projectile mass insensitivity for processes leading to the C_3^+-C_{11}^+ fragments as due to similarities in nuclear as well as electronic energy transfers in the glancing collisions, while the sensitivity to the projectile mass for the more distant collisions leading to the $C_{60/70-2m}^{3+}$ $(m = 1–7)$ fragments could not consistently be described with the simple Monte Carlo calculations. This shortcoming is most likely due to inadequate descriptions of electronic processes in more distant ionizing collisions with multiply charged ions. This stresses the importance of more advanced quantum mechanical approaches, similar to the ones performed by Kunert and Schmidt [11] who used Density Functional Theory in a dynamic approach, in order to further elucidate the complex energy transfer mechanisms in collision systems involving *multiply* charged projectile ions.

References

1. E.E.B. Campbell, F. Rohmund, Rep. Prog. Phys. **63**, 1061 (2000)
2. E.E.B. Campbell, *Fullerene Collision Reactions* (Kluwer Academic Publishers, 2003)
3. S. Martin, L. Chen, A. Denis, J. Désesquelles, Phys. Rev. A **57**, 4518 (1998)

4. R. Vandenbosch, B.P. Henry, C. Cooper, M.L. Gardel, J.F. Liang, D.I. Will, Phys. Rev. Lett. **81**, 1822 (1998)
5. H. Cederquist, A. Fardi, K. Haghighat, A. Langereis, H.T. Schmidt, S.H. Schwartz, J.C. Levin, I.A. Sellin, H. Lebius, B.A. Huber, M.O. Larsson, P. Hvelplund, Phys. Rev. A **61**, 022712 (2000)
6. A. Reinköster, U. Werner, N.M. Kabachnik, H.O. Lutz, Phys. Rev. A **64**, 023201 (2001)
7. B. Walch, C.L. Cocke, R. Voelpel, E. Salzborn, Phys. Rev. Lett. **72**, 1439 (1994)
8. U. Thumm, A. Bárány, H. Cederquist, L. Hägg, C.J. Setterlind, Phys. Rev. A **56**, 4799 (1997)
9. H. Zettergren, H.T. Schmidt, H. Cederquist, J. Jensen, S. Tomita, P. Hvelplund, H. Lebius, B.A. Huber, Phys. Rev. A **66**, 032710 (2002)
10. J. Jensen, H. Zettergren, H.T. Schmidt, H. Cederquist, S. Tomita, S.B. Nielsen, J. Rangama, P. Hvelplund, B. Manil, B.A. Huber, Phys. Rev. A **69**, 053203 (2004)
11. T. Kunert, R. Schmidt, Phys. Rev. Lett. **86**, 5258 (2001)
12. J. Jensen, H. Zettergren, A. Fardi, H.T. Schmidt, H. Cederquist, Nucl. Intrum. Meth. Phys. Res. B **205**, 643 (2003)
13. H. Cederquist, J. Jensen, H.T. Schmidt, H. Zettergren, S. Tomita, B.A. Huber, B. Manil, Phys. Rev. A **67**, 062719 (2003)
14. S. Díaz-Tendero, M. Alcamí, F. Martín, Phys. Rev. Lett. **95**, 013401 (2005)
15. A. Rentenier, A. Bordenave-Montesquieu, P. Moretto-Capelle, D. Bordenave-Montesquieu, J. Phys. B: At. Mol. Opt. Phys. **37**, 2429 (2004)
16. A Rentenier, A. Bordenave-Montesquieu, P. Moretto-Capelle, D. Bordenave-Montesquieu, J. Phys. B: At. Mol. Opt. Phys. **37**, 2455 (2004)
17. L. Chen, J. Bernard, A. Denis, S. Martin, J. Désesquellles, Phys. Rev. A **59**, 2827 (1999)
18. S. Martin, L. Chen, R. Bredy, J. Bernard, M.C. Buche-Paulizac, A. Allouche, J. Désesquelles, Phys. Rev. A **66**, 063201 (2002)
19. P. Hvelplund, L.H. Andersen, H.K. Haugen, J. Lindhard, D.C. Lorentz, R. Malhotra, R. Ruoff, Phys. Rev. Lett. **69**, 1915 (1992)
20. A. Langereis, J. Jensen, A. Fardi, K. Haghighat, H.T. Schmidt, S.H. Schwartz, H. Zettergren, H. Cederquist, Phys. Rev. A **63**, 062725 (2001)
21. S. Martin, L. Chen, R. Brédy, J. Bernard, A. Salmoun, B. Wie, Phys. Rev. A **69**, 043202 (2004)
22. O.B. Firsov, Sov. Phys. JETP **36**, 1076 (1959)
23. M.C. Larsen, P. Hvelplund, M.O. Larsson, H. Shen, Eur. Phys. J. D **5**, 283 (1998)
24. T. Schlathölter, O. Hadjar, R. Hoekstra, R. Morgenstern, Phys. Rev. Lett. **82**, 73 (1999)
25. T. Schlathölter, O. Hadjar, J. Manske, R. Hoekstra, R. Morgenstern, Int. J. Mass Spectrom. **192**, 245 (1999)
26. T. Schlathölter, R. Hoekstra, R. Morgenstern, J. Phys. B: At. Mol. Opt. Phys. **31**, 1321 (1998)
27. A. Reinköster, B. Siegmann, U. Werner, B.A. Huber, H.O. Lutz, J. Phys. B: At. Mol. Opt. Phys. **35**, 4989 (2002)
28. G. Javahery, S. Petrie, J. Wang, D.K. Bohme, Chem. Phys. Lett. **195**, 7 (1992)
29. V. Blagojevic, S. Petrie, D.K. Bohme, Int. J. Mass Spectrom. **233**, 33 (2004)
30. S. Martin, R. Brédy, J. Bernard, J. Désesquelles, L. Chen, Phys. Rev. Lett. **89**, 183401 (2002)